Revealing of InP multi-layer stacks from KPFM measurements in the dark and under illumination

Mattia da Lisca, James P. Connolly, J Alvarez, Karim Mekhazni, Nicolas Vaissiere, Jean Decobert, Jean-Paul Kleider

EPJ Photovoltaics **13**, 19 (2022)

https://doi.org/10.1051/epjpv/2022017

Available online at:
www.epj-pv.org

Special Issue on 'Recent Advances in Spectroscopy and Microscopy of Thin-films Materials, Interfaces, and Solar Cells 2021', edited by A. Vossier, M. Gueunier-Farret, J.-P. Kleider and D. Mencaraglia

REGULAR ARTICLE OPEN ACCESS

Revealing of InP multi-layer stacks from KPFM measurements in the dark and under illumination

Mattia da Lisca[1,2,3,*], James P. Connolly[1,2,3], José Alvarez[1,2,3], Karim Mekhazni[4], Nicolas Vaissiere[4], Jean Decobert[4], and Jean-Paul Kleider[1,2,3]

[1] Institut Photovoltaïque d'Ile de France, 30 Route Départementale 128, 91120 Palaiseau, France
[2] Université Paris-Saclay, CentraleSupélec, CNRS, Laboratoire de Génie Electrique et Electronique de Paris, 91192 Gif-sur-Yvette, France
[3] Sorbonne Université, CNRS, Laboratoire de Génie Electrique et Electronique de Paris, 75252 Paris, France
[4] III-V Lab, 1 Avenue Augustin Fresnel, 97167 Palaiseau, France

Received: 28 March 2022 / Received in final form: 18 July 2022 / Accepted: 28 July 2022

Abstract. Solar cells are complex devices, being constituted of many layers and interfaces. The study and the comprehension of the mechanisms that take place at the interfaces is crucial for efficiency improvement. This paper applies Kelvin probe force microscopy (KPFM) to study materials and interfaces with nanometer scale imaging of the surface potential in the dark and under illumination. KPFM measurements are highly sensitive to surface states and to the experimental measurement environment influencing the atomic probe operating conditions. Therefore, in order to develop a quantitative understanding of KPFM measurements, we have prepared a dedicated structured sample with alternating layers of InP:S and InP:Fe whose doping densities were determined by secondary-ion mass spectroscopy. We have performed KPFM measurements and shown that we can spatially resolve 20 nm thick InP layers, notably when performed under illumination which is well-known to reduce the surface band-bending.

Keywords: Kelvin probe force microscopy / III-V multilayer stack / surface photovoltage

1 Introduction

In the context of global climate heating, the use of low greenhouse gas power sources is a priority [1], amplified by a continuous growing energy consumption. Solar energy is recognized as one of the most promising and stable renewable energy sources and national governments are providing incentives for its development [2].

Over the last decade, substantial advances in material and solar cell device engineering have produced significant progress in the development of photovoltaic (PV) technologies. As a result, solar cells have evolved into elaborate structures with numerous layers and interfaces.

This continuous and rapid progress of the various PV technologies is largely related to the improvement of the quality of the active layers and interfaces. The characterization of the different building blocks constituting the devices increasingly requires the capacity to carry out local analyses at the nanoscale level yielding information on electronic properties of materials and interfaces.

In particular, the doping plays a key role since it can strongly impact the electrical, optical, and structural properties of a material and device performance. In this regard, a multitude of techniques can be applied for its characterization. Secondary-ion mass spectrometry (SIMS) and electron holography in transmission electron microscopy (TEM) can be used for this purpose with a resolution of the order of 10 nm [3]. Nevertheless, technical limitations can arise in detecting low dopant concentrations (10^{14} cm^{-3}) and thin layers (nm) as in the case of SIMS [4]. Challenging sample preparation is often required, making these methods time consuming and destructive.

Scanning probe microscopy (SPM) is another approach that allows the investigation of the doping thanks to the wide variety of AFM electrical extensions that have been developed to perform a broad range of characterizations at the nanoscale [5]. Specifically, scanning spreading resistance microscopy (SSRM) [6], scanning capacitance microscopy (SCM) [7] and Kelvin probe force microscopy (KPFM) [8] are suitable for this purpose.

SSRM and SCM measure the local resistivity and capacitance of a semiconductor material, whereas KPFM is valuable for the study of work functions and surface potential.

* e-mail: mattia.dalisca@ipvf.fr

Nonetheless, SSRM is classified as destructive method since high normal forces are applied in order to penetrate the oxide layer and specially to keep a stable electrical contact, while SCM requires an oxide layer on the surface and modelling to obtain quantitative results [9]. Conversely, KPFM is a non-contact method which does not require specific sample preparation and has been used to detect and contrast doping concentrations in a range from 10^{14} to 10^{19} cm^{-3} [4,9–11].

In order to perform successful KPFM measurements, a low surface roughness is essential to obtain high-quality images since surface inhomogeneities can cause a topographical image imprint on the potential image. Furthermore, other factors, including the presence of electrically active surface defects, the experimental measurement environment, and the AFM probe operating conditions, can affect KPFM measurements [12,13].

For this reason, we have prepared and investigated an ambitious sample by the number of existing layers in order to obtain a quantitative comprehension of KPFM measurements. The specimen consists of an alternated repetition of 42 layers of InP:S and InP:Fe.

Impurities of S are known to form shallow donors in InP [14]. Moreover, they can efficiently reduce the dislocation density produced in the crystal during the growth process. Dislocation-free InP crystals can be used as substrates to fabricate devices such as lasers and photodiodes with high reliability and high performance [15]. InP:S-based solar devices have been reported in the literature. In particular, Faur et al. [16] reported a p^+n (Cd,S) heterojunction InP solar cells for space applications and a InP:S/AlInAs:C tunnel junction, presented by the III-V Lab group [17], has been successfully produced and used to fabricate InP/InGaAs tandem solar cells [18].

Undoped InP crystals always contain unintentional impurities due to the growth processes. In particular, the non-intentionally doped (nid) InP layers fabricated at III-V Lab usually present an intrinsic n-type doping in the order of 10^{15} cm^{-3} that results in shallow donor energy levels within the energy gap.

Fe doping provides acceptor levels in the mid-gap region of InP which compensate shallow donors and thus produce a semi-insulating (SI) material [19]. InP:Fe is generally used as substrate for the growth of Si/InP with low dislocation density for III–V integration on Si [20].

Therefore, the investigation of the surface properties at the nano-scale of InP:S and InP:Fe is of great interest, as is the need of quantitative analysis of the experimental data.

The layers in our sample present different thickness from 20 nm to 200 nm in order to evaluate the spatial resolution achievable in ambient conditions KPFM and the reproducibility of the measurement.

To perform the characterization of interfaces, thicker layers in the order of over 1 μm would be more suitable in order to better analyze the surface properties of the two semiconductors materials and the band-bending at the interfaces. However, we are interested specifically in materials for III-V solar cell applications, for which layer thicknesses are typically less than a micron, and of the order of tens to hundreds of nm. In particular, III-V solar devices belong to the PV technology of thin and ultra-thin films in which the presence of layers with width comparable to the one of the layers in our sample are very common, including in particular window and etch stop layers [21].

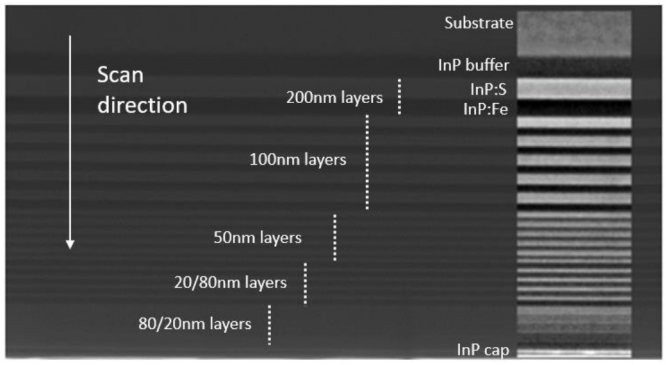

Fig. 1. SEM image of the InP:S and InP:Fe sample surface. The image was edited to highlight with the gray and black color the InP:S and InP:Fe layers, respectively. The first two layers represent the substrate and the nid buffer layer.

In a complete solar cell, the KPFM analysis of such interfaces may reveal the presence of unexpected potential barriers which hinder the extraction of the photogenerated charges [22]. Consequently, the experimental demonstration of the sensitivity of the KPFM technique to the narrower layers can play a crucial role in the investigation and comprehension of the local surface properties and charge transport mechanisms at the interfaces.

2 Experiment

2.1 Sample preparation

The InP stack was epitaxially grown using MOVPE process in an AIXTRON Close-Coupled Showerhead reactor ($6 \times 2''$) at a surface temperature of 580 °C on a n-type InP substrate from AXT whose doping is typically in the range of $3–5 \times 10^{18}$ cm^{-3} with a thickness of 500 μm. The growth rate and the surface temperature of the InP layers are determined using an in-situ Laytec EpiCurve TT tool by employing a laser reflectometer with a laser wavelength of 980 nm.

Trimethylindium (TMIn) and phosphine (PH_3) are the source materials mixed to hydrogen (H_2) as a carrier gas. Hydrogen sulfide (H_2S) and ferrocene (Cp_2Fe) compounds are used respectively for n-type InP:S and semi-insulating InP:Fe layers. After the synthesis, the S and Fe concentrations were determined by secondary-ion mass spectrometry (SIMS) and found to be equal to 2×10^{19} cm^{-3} and 9×10^{16} cm^{-3} for the InP:S and InP:Fe layers, respectively. The Fe doping concentration is close to optimal since adding more Fe to the growth will only form FeP precipitates that degrade the crystalline quality without adding electrical benefits.

The layers stack is enclosed by two 200 nm-thick non-intentionally doped InP layers called buffer and cap. Inside the stack and starting from the epitaxial interface toward the surface, two 200 nm-thick layers of InP:S/InP:Fe were grown plus four loops of five repetitions by varying the thickness of each layer as follows: 100/100, 50/50, 80/20 and 20/80 nm for InP:S/InP:Fe (see Fig. 1 for a SEM image of the sample).

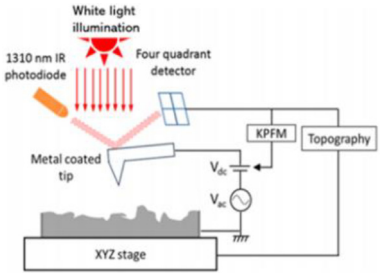

Fig. 2. Schematic diagram of KPFM system used in this analysis. While an AC + DC potential is applied, the KPFM tip scans across a surface. The AC signal is sinusoidal with a frequency that equals the mechanical resonance of the cantilever. The four-quadrant detector gives feedback in order to minimize cantilever oscillation modifying the DC signal providing the sample surface potential relative to that of the tip.

Prior to the KPFM analysis, a surface cleaning was carried out with the purpose of removing the expected oxide at the surface. In particular, a chemical treatment based on sequential ultrasonic baths of acetone, ethanol, and deionized water was used. The sample was then placed in 1% HF solution for 30 seconds to chemically etch the top oxide layer. This step was followed by a rinsing with deionized water and drying in air.

2.2 Kelvin probe force microscopy

KPFM measures the contact potential difference (V_{CPD}) between a conducting AFM tip and a sample, which is defined as:

$$V_{\mathrm{CPD}} = V_{\mathrm{sample}} - V_{\mathrm{tip}} \quad (1)$$

where V_{sample} and V_{tip} are the electrostatic potential values at the surface of the sample and of the tip, respectively. The V_{CPD} between a probe tip and a sample surface is measured using a two-step scan. Topographical data are collected on the first pass, and the V_{CPD} is evaluated during the second pass while keeping the tip at a predefined constant height above the sample surface. The V_{CPD} is imaged by measuring the DC voltage required to compensate for the electrostatic force which determines the KPFM signal [8]. KPFM was performed using a scanning probe microscopy system from AIST-NT (TRIOS platform) in ambient conditions, and operated in frequency-modulation KPFM (FM-KPFM) using a two-pass scanning mode where the second pass was performed at a constant distance of 10 nm from the sample surface (see Fig. 2 for a schematic of our KPFM setup). While in amplitude modulation KPFM (AM-KPFM) the force is directly evaluated, in FM-KPFM the gradient of the force is analyzed. When compared to standard AM-KPFM analysis, FM-KPFM has a better spatial resolution in detecting the surface potential. The long-ranged electrostatic interactions of the cantilever are reduced and thus the effect of parasitic capacitances is mitigated [23].

Note that the laser beam-based deflection system in our AFM employs a laser wavelength at 1310 nm that minimizes the possible photoelectric interactions with the sample [24]. n^{+}-Si ARROW EFM tips with a conductive Pt/Ir coating at a resonance frequency of 75.6 kHz were used.

KPFM measurements were performed in dark conditions and under illumination on the cross-section of the sample. For our study, the white light coming from the camera connected to the microscope was used in order to have a uniform illumination of the entire surface cross-section.

3 Results

3.1 KPFM cross-sectional investigation

KPFM is a surface investigation technique, and therefore, the presence of a native oxide surface layer on top can influence the measurements causing the detection of a deceptive V_{CPD} value and, in extreme case, hide the surface features of interest. Preliminary results (not shown) confirmed the presence of an oxide layer which prevents the detection of the underlying surface potential of the InP:S and the InP:Fe layers. The approach described in Section 2.1 was attempted in order to remove this surface oxide.

The topography and the V_{CPD} images obtained from KPFM investigation in dark conditions after the chemical surface cleaning are reported in Figures 3a and 3b, respectively.

According to Figure 1, the dark regions in the V_{CPD} image (see Fig. 3b) represent the InP:S layers while the InP:Fe ones are denoted by the bright lines.

During the KPFM analysis, the tip scanned vertically the surface of the sample from the InP substrate to the sample edge which caused the imprint of vertical lines in the images, which is especially observed in Figure 3b. Note that the origin (0;0) is identified as a point in the InP substrate and moving along the positive direction of the Y axis, one will reach the end of the sample.

The topography image (Fig. 3a) indicates that a smooth and homogeneous surface was provided by the HF treatment and a complete detection of the stack in the V_{CPD} image was achieved. The topography revealed a dip in its middle (from 3 μm to 8 μm along the X axis) of 10 nm which cause can be attributed to the cleaving process. Nonetheless, the topographic features are barely visible and thus the nature of the physical contrast can be attributed to a pure dopant effect excluding the topography imprint on the V_{CPD} map.

The progression of the V_{CPD} profiles along region 1 and 2 identified in the V_{CPD} map are reported in Figure 4. These two regions are compared in particular because they show different contrasts for the 100 nm thick layers. For this reason, several vertical profiles around regions 1 and 2 were extracted from the topography image and compared (not shown). All the profiles showed the same progression definitively excluding the presence of topographic artifacts imprinted in the V_{CPD} image. Therefore, the reason for the discrepancy between these two regions is not clear at this stage but may be related either to the deoxidation treatment or to the cleaving process. The factors which influence the V_{CPD} will be explored in more detail in Section 4.1.

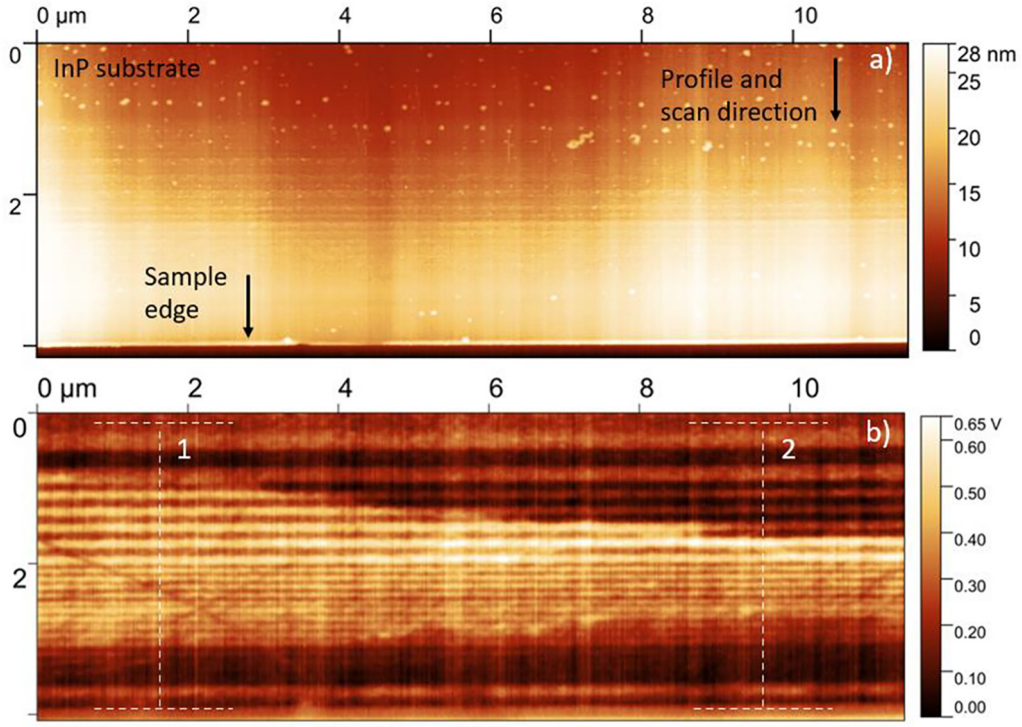

Fig. 3. KPFM measurement in ambient conditions on the surface cross-section of the InP sample in dark conditions. (a) Topography image of the cross-section of the InP sample after chemical removal of the oxide layer. (b) The V_{CPD} image measured during the second pass. Two regions with different V_{CPD} progression were detected and labelled with 1 and 2. The resolution of the images is set to 1024×1024 pixels per point.

The examination of the V_{CPD} profile allows a first qualitative analysis. The width of the peaks is comparable to the one of the layers presented in Section 2.1. This represents consistent evidence of the great sensitivity of the KPFM technique to the local doping concentration, already reported in a number of publications [4,13].

The intensity of the peaks changes with the width of the layers. In particular, considering the profile extrapolated from region 1, the ΔV_{CPD} was calculated among adjacent InP:S and InP:Fe with same thickness. Note that, in the case of the 100, 50 and, 20/80 regions, which comprise a repetition of 10 layers each, an averaged ΔV_{CPD} value is reported. Specifically, the ΔV_{CPD} is 230 mV for the 200 nm wide layers, 185 mV for the 100 nm wide layers, 78 mV for the 50 nm wide layers and 52 mV for the 20/80 nm (InP:S/InP:Fe) wide layers, respectively. In the last region, the 80/20nm (InP:S/InP:Fe), the 20 nm wide InP:Fe layers are poorly detected and the evaluation of a clear ΔV_{CPD} is not achieved.

The two uneven 20/80 and 80/20 InP:S/InP:Fe stacks near the cap layer present a different resolution in the detection of the 20 nm thick layers. In the 20/80 region, the InP:S layers are still reasonably well detected despite being only 20 nm thick, whereas the 20 nm InP:Fe layers in the 80/20 region are not well-resolved although they present the same thickness, this is especially evident in the profile along region 1. Therefore, the poor detection of the 20 nm thick InP:Fe layers cannot be only related to the limitations of resolution of ambient conditions KPFM. In particular, since KPFM demonstrated a strong dependence on the local doping concentration, in the 80/20 region, where the InP:S layers are four time bigger than the InP:Fe, the contribution to the V_{CPD} signal of the InP:S layers tends to dominate over the one from the InP:

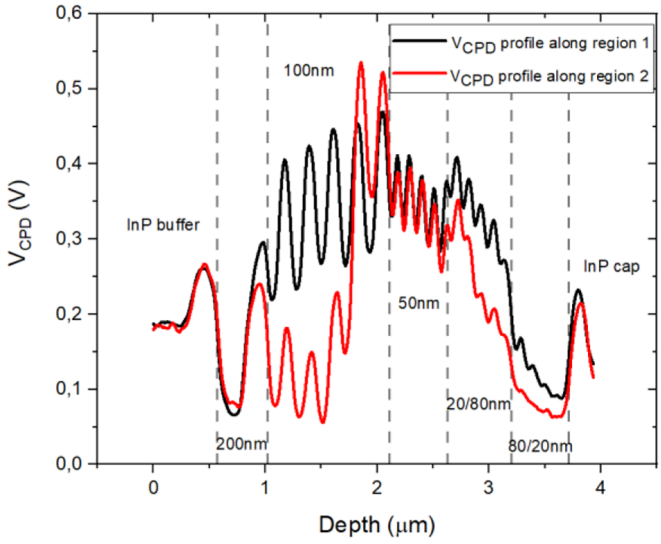

Fig. 4. Vertical profiles of the two regions labeled with 1 and 2 identified in the V_{CPD} map in Figure 3b. The profiles correspond to the regions identified by the two dotted white segments, and they were obtained by averaging over a width of 128 points.

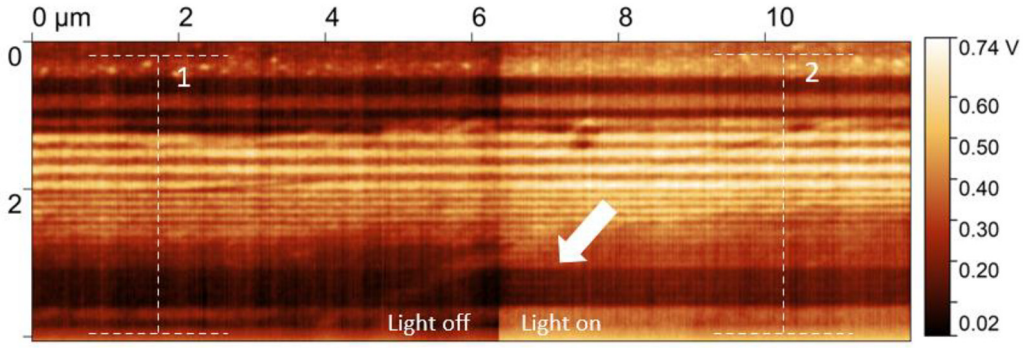

Fig. 5. KPFM measurement in ambient conditions on the surface cross-section of the InP sample in dark conditions (left half) and under white light illumination (right half). The resolution of the image is set to 1024 ×1024 pixels per point.

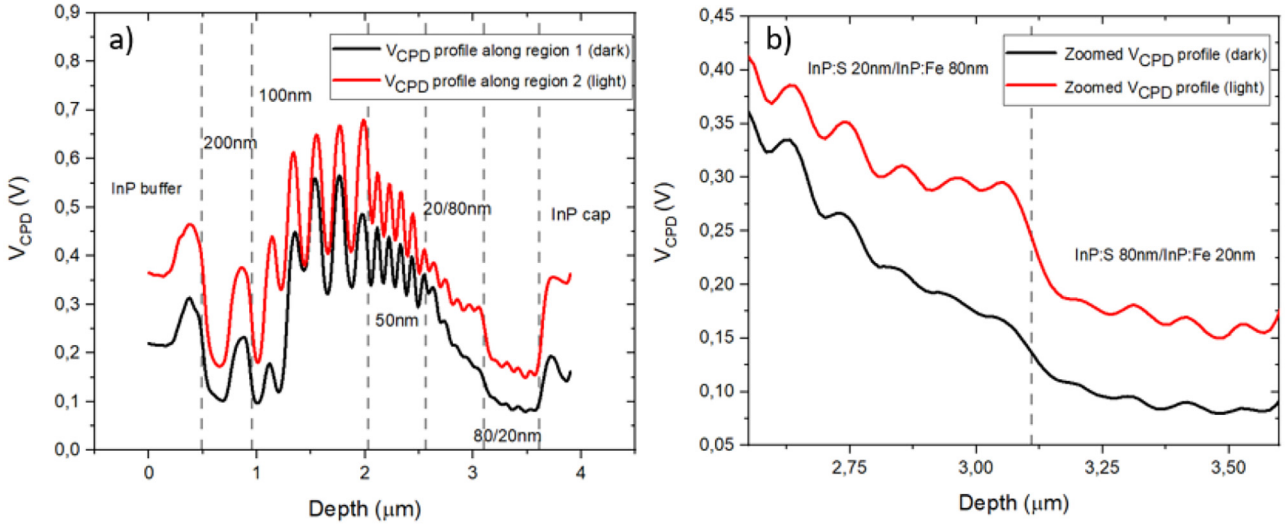

Fig. 6. (a) Vertical profiles extrapolated from the dark and light regions of Figure 5. (b) Vertical profiles extrapolated from the dark and light regions zoomed on the 20 and 80 nm layers. Note that, the profiles correspond to the regions identified by the two dotted white segments in Figure 5.

Fe due to the large difference in dimension and in the doping concentration between the two layers. As a matter of fact, the V_{CPD} value in the 80/20 region is comparable to the one measured for the 200 nm InP:S thick layer. This is also consistent with the fact that the 20 nm thick InP:S layers in the 20/80 region are reasonably well-resolved.

Nonetheless, from this first stage analysis, it is clear that an adequate detection of the narrower layers in the V_{CPD} image becomes more challenging. This is related to the spatial limitations of the KPFM measurement setup. In fact, approaching the 20 nm wide layers, their dimension become comparable to that of the probe (10 nm). This part will be discussed in Section 4.1.

Interestingly, InP:S and InP:Fe layers of different but similar thickness tend to show different V_{CPD} despite, respectively, being of the same S or Fe doping. This suggests that minor changes in thickness can lead to more significant difference in V_{CPD} than one might expect from the position of the bulk Fermi level. The principal reason for this behavior is the fact that successive InP:S and InP:Fe layers form homojunctions, and therefore the extension of the space charge regions depends on the thickness of the layers. This aspect will be fully addressed in Section 4.2.

3.2 KPFM under illumination: the effect of the light

In order to evaluate the effect of the illumination on the sample, KPFM measurements were started in dark conditions (region 1) and completed under illumination (region 2); the corresponding V_{CPD} map is reported in Figure 5.

A significant contrast improvement is observed along all the structure, as shown by the red profile in Figure 6a. The peaks related to the illuminated region are more pronounced with respect to ones extrapolated from the V_{CPD} values obtained in dark conditions. In particular, the 20 and 80 nm wide layers in the last two regions are only

visible and well-distinguished after the application of the light, as highlighted by the more prominent red peaks in the zoomed vertical profiles reported in Figure 6b.

The acquisition of the V_{CPD} image in dark conditions ($V_{CPD/dark}$) and under illumination ($V_{CPD/light}$) enables the evaluation of the surface photovoltage (SPV). The SPV is obtained from the difference between $V_{CPD/light}$ and $V_{CPD/dark}$ [25]:

$$SPV = V_{CPD/light} - V_{CPD/dark}. \quad (2)$$

Since the surface potential of the tip is assumed to be unaffected by illumination, the difference between $V_{CPD/light}$ and $V_{CPD/dark}$ is indeed equal to the change in surface potential of the sample between illumination and dark, which defines the surface photovoltage.

From Figure 6a we observe that the SPV is positive all along the structure in the order of hundreds of mV for both the InP:S and InP:Fe layers, which is unexpected from the bulk properties of InP:S. In particular, for the highly-doped InP:S, we expect a positive SPV but close to 0 and probably below detection limits under the low light intensity illumination used in the experiment [26]. This will be discussed further in Section 4.3.

4 Discussion

In this section the principal factors which affect KPFM measurements will be addressed in order to develop a methodology of analysis and apply it to the experimental results.

4.1 Sample preparation and KPFM experimental conditions

We have described in Section 3.1 that different V_{CPD} values were detected for the two different regions identified in Figure 3b despite belonging to the same scan and being distant only a few micrometers.

Several factors can influence KPFM measurements leading to this experimental evidence. In particular, it is well-documented in literature [25] that the cleavage procedure induces surface defects which strongly impact the V_{CPD}. In addition, the deoxidation procedure may not be very efficient, causing a nonuniform removal of the surface oxide. Note that, the role of surface defects in influencing the V_{CPD} will be addressed in Section 4.3.

A further aspect to consider concerns the experimental conditions. KPFM measurements were performed in ambient conditions, and this promotes the oxidation of the surface and the adsorb of water molecules on the surface coming from the humidity in air [27]. These aspects together may lead to surface inhomogeneities which locally affect V_{CPD} and result in variations in otherwise constant bulk material.

In addition, the state of the tip must be considered. Tip contamination is likely to happen due to the pollutants which may be present on the sample surface causing a variation of the tip surface potential.

For these reasons, the reproduction of identical V_{CPD} profiles along the structure analyzing different regions is a challenging task. These inhomogeneities are also visible in the dark V_{CPD} profile reported in Figure 6a. Although it is not directly comparable with the two dark V_{CPD} profiles in Figure 4, it is evident that it shows the same qualitative V_{CPD} progression.

Furthermore, we have pointed out how the ΔV_{CPD} between the InP:S and InP:Fe layers decreases with their width. This phenomenon relates to the tip-averaging effect due to the long-range nature of the electrostatic force. Since the layers are particularly narrow and alternate, the KPFM tip, working at tip-surface distance of 10 nm, can sense multiple layers at the same time resulting in the detection of an averaged V_{CPD}. In our case, this effect is especially relevant since the dimension of the narrower layer (20 nm) is comparable to the radius of the tip (10 nm). The tip-averaging effect largely affects the lateral resolution and the measured KPFM signal, even for very small tip-sample distance (5 nm) [28]. This is particularly observed in ambient conditions KPFM measurements, where typical tip-surface distances are of the order of tens of nm due to the amplitude of the vibrating tip required to obtain a reasonable signal-to-noise ratio.

4.2 Effect of the space charge on the V_{CPD}

As mentioned in Section 3.1, successive layers of InP:S and InP:Fe form homojunctions with layer thicknesses ranging from 200 nm to 20 nm. Note that, the width of the space charge is determined by the doping concentration, and that a larger depletion zone is expected in the InP:Fe layers that have less Fe impurities as compared to the S concentration in the InP:S layers. Given the thicknesses of the fabricated layers, it can be expected that all InP:Fe layers are depleted and that "the end" of the space charge is never reached, hence limiting the V_{CPD} contrast.

As anticipated in Section 1, Fe impurities introduce acceptor levels in the mid-gap region of InP that compensate residual shallow donors making the InP semi-insulating. The Fe doping thus is responsible for increasing the resistivity of the InP material. The literature reports that introducing a concentration of the order of 10^{16} cm^{-3}/10^{17} cm^{-3} of Fe impurities results in resistivities of InP reaching values of the order of 10^7/10^8 Ωcm with an associated residual majority charge carrier density (electrons) of 10^7/10^6 cm^{-3} [29].

For this reason, in order to replicate the band profiles of the structure, we have used Silvaco software [30] to model a n^+n homojunction specifying a doping concentration of 2×10^{19} cm^{-3} and 10^6 cm^{-3} for the InP:S and InP:Fe layers respectively. The energy variation of the valence and conduction bands along the structure is reported in Figure 7a along with the Fermi level (E_F). Note that the Fermi level E_F is pinned to the conduction band due to the higher doping concentration of S with respect to the InP effective conduction band density of states (5.7×10^{17} cm^{-3}).

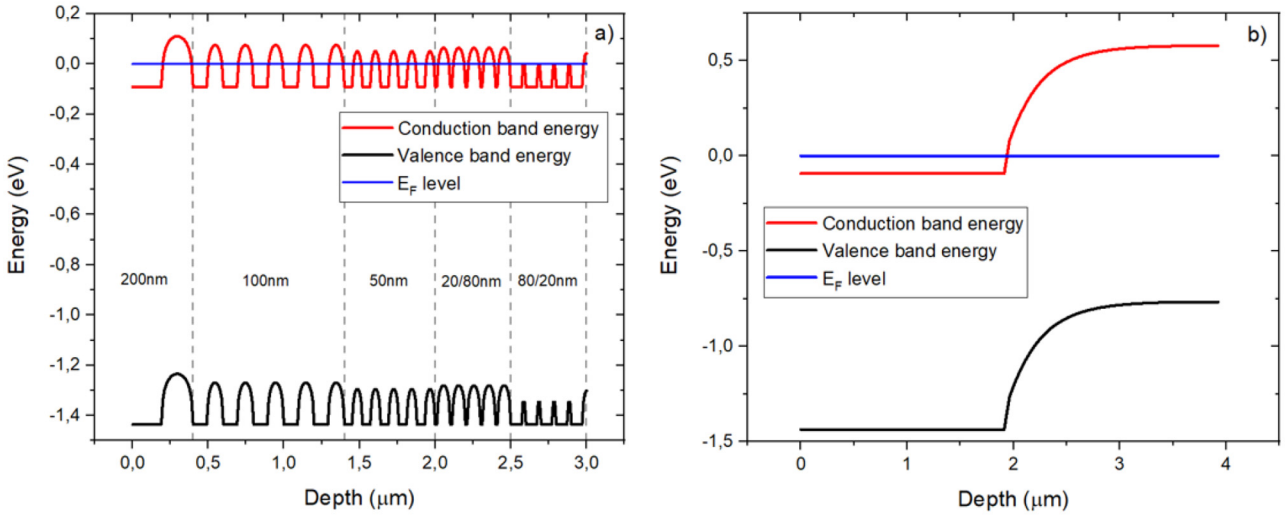

Fig. 7. Progression of the valence and conduction band energies (a) along the InP:S/InP:Fe structure and (b) along a hypothetical 2 μm thick InP:S/InP:Fe homojunction. The valence and conduction bands are represented by the black and red color, respectively. The Fermi level (E_F) level is also reported in blue.

As mentioned at the beginning of this section and showed in Figure 7a, the thickness of the layers has a direct impact on the width of the space charge region among the homojunctions. As comparison, the energy bands profile variation of a hypothetical 2 μm thick InP:S/InP:Fe structure constituted by only two layers was simulated maintaining the same parameters and reported in Figure 7b. In this case, InP:Fe bands finally reach the flat-band condition showing that the space charge region extends in the InP:Fe for around 1 μm.

In the case of our sample, the space charge region covers the entire width of the InP:Fe layers. This has a direct effect on the V_{CPD} values. In particular, the InP:Fe layers are fully depleted, but the number of charges in the space charge region depends on the thickness of the layers revealing how decreasing the thickness of the layers decreases the corresponding potential variation and therefore the V_{CPD}.

Moreover, the bands evolution of this simpler structure points out also that the InP:Fe layers are depleted from both sides since each layer is in contact with two different InP:S layers. This is the reason why the InP:Fe bands in our sample structure are symmetric with respect to an axis passing through half of the thickness.

4.3 Effect of the illumination on the V_{CPD}

On a cleaved semiconductor surface, surface states might be present due to the termination of lattice periodicity at the surface, thus forming dangling bonds of surface atoms with energies deep in the bandgap. These surface states will pin the Fermi level and cause downward (upward) band-bending from the bulk to the surface in a p-type (n-type) semiconductor [31].

Under illumination, a dopant concentration dependent SPV is produced by the diffusion of photo-generated carriers towards the surface, which counteracts the defect-induced band-bending variations [25]. In the case of upward surface band bending in an n-type semiconductor, photogenerated electrons are repelled from the surface, while photogenerated holes drift towards the surface, balancing the negative charges corresponding to ionized surface defects, as exemplified in Figure 8.

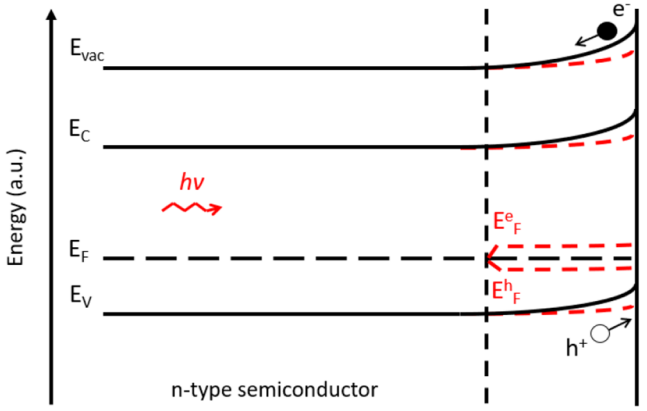

Fig. 8. Representation of the energy bands profile in a n-type semiconductor in dark conditions and under illumination depicted by black solid lines and red dashed lines, respectively. E^e_F and E^h_F represent possible profiles for the quasi-Fermi levels for electron and holes, respectively.

The consequence is a reduction of net surface of band-bending and an increase of surface potential, as follows a positive SPV. In the same way, for p-type semiconductors, the downward band bending is reduced under illumination, producing a decrease of surface potential, and therefore a negative SPV. The sign of SPV can therefore be used to determine the doping character of semiconductor materials [32]. However, in case of pn junctions, the SPV can also include the contribution of an open-circuit voltage due to the splitting of the quasi-Fermi levels of electrons and

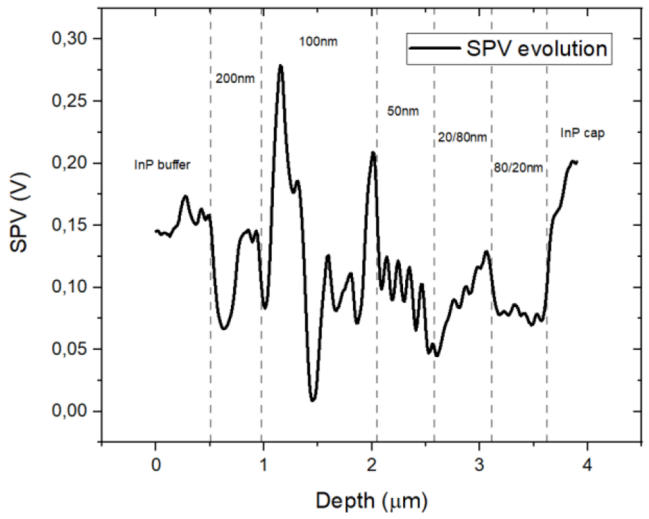

Fig. 9. SPV evolution along the structure calculated from the dark and light profiles showed in Figure 6a applying equation (2).

holes [33].

The light-induced surface band-bending reduction explains the significant contrast improvement in the V_{CPD} image reported in Figure 5 and described in Section 3.2.

For highly doped semiconductors in the absence of surface states a very low SPV signal is expected after the illumination by low light intensity [25]. Moreover, experiments performed on silicon wafers with varying doping densities have shown that, overall, the SPV signal tends to be larger for low doping densities [33].

From Figure 9 we observe that the SPV is positive all along the structure in the order of hundreds of mV for both the InP:S and InP:Fe layers with variations in the order of tens of mV and it can be noticed that the SPV is indeed larger in the InP:Fe layers.

The SPV sign is in good agreement with what is expected for the InP:S and InP:Fe layers. However, in terms of SPV intensity, a significant positive SPV is detected in the highly doped n-type InP:S layers which is surprising considering the low light intensity illumination.

Nonetheless, this can be explained by the presence of a large surface states density caused by surface defects inducing significant upward band-bending even in highly doped layers [13,25]. Modelling is required to have a more quantitative analysis of the SPV experiment on these multilayer stacks, in particular to study the combined effect of quasi-Fermi level splitting and surface state densities, and this will be the objective of future work.

5 Conclusions

We have shown that KPFM is a valuable technique to investigate a InP:S and InP:Fe multilayer stack with high spatial resolution in ambient conditions. In particular, KPFM provided the detection of the entire stack after a surface deoxidation by an HF based chemical treatment.

KPFM revealed a strong dependence on the local doping concentration providing a complete detection of the InP:S and InP:Fe layers which exhibited different color contrast in the V_{CPD} image. Moreover, we showed that the V_{CPD} contrast between the InP:S and InP:Fe layers could even be significantly improved when KPFM measurements were performed under illumination.

The analysis of V_{CPD} profiles shows that InP:S and InP:Fe layers of different but similar thickness tend to show different V_{CPD}, which can be attributed to the band-bending induced by the space charge due to the different doping densities of the InP:S and InP:Fe layers, as shown in the simulated energy bands progression.

The V_{CPD} profiles extrapolated from different regions of the same scan showed the same V_{CPD} qualitative progression but presented minor variations. For this reason, a thorough analysis and description of the many factors that influence KPFM measurements has been performed in order to investigate these differences.

Finally, the analysis of the SPV along the structure pointed out that a positive SPV in the order of hundreds of mV was detected even for the InP:S layers, which is surprising considering the bulk properties of this material. Nonetheless, this can be justified by a large surface state defect density responsible of producing significant upward band bending. An exhaustive analysis of the effect of surface defects on the SPV will be the object of a future work.

References

1. M. Azhar Khan et al., Renew. Sustain. Energy Rev. **29**, 336 (2014)
2. E. Kabir et al., Renew. Sustain. Energy Rev. **82**, 894 (2018)
3. D. Tsurumi et al., Jpn. J. Appl. Phys. **51**, 106503 (2012)
4. U. Gysin et al., Microelectr. Eng. **160**, 18 (2016)
5. R. Berger et al., Macromol. Rapid Commun. **30**, 1167 (2009)
6. P. Eyben et al., J. Vac. Sci. Technol. B **20**, 471 (2002)
7. K. Kimura et al., Appl. Surf. Sci. **210**, 93 (2003)
8. W. Melitz et al., Surf. Sci. Rep. **66**, 1 (2011)
9. P. De Wolf et al., J. Vacuum Sci. Technol. B **18**, 361 (2000)
10. H. Shin et al., J. Appl. Phys. **77**, 1888 (1995)
11. A. K. Henning et al., J. Appl. Phys. **77**, 1888 (1995)
12. Y. Rosenwaks et al., Phys. Rev. B **70**, 085320 (2004)
13. Th. Glatzel et al., Mater. Sci. Eng. B **102**, 138 (2003)
14. M.M. El-Nahass et al., Physica A **402**, 216 (2014)
15. F. Zafar et al., JT Proc. R. Soc. A **472**, 20150804 (2016)
16. M. Faur et al., IEEE 1st World Conference on Photovoltaic Energy Conversion **2**, 2211 (1994)
17. S. Soresi et al., Phys. Stat. Solidi (a) **215**, 1700427 (2018)
18. S. Soresi et al., InP based tandem solar cells integrated onto Si substrates by heteroepitaxial MOVPE, Université Montpellier, 2018
19. LN. Alyabyeva et al., Sci. Rep. **7**, 7360 (2017)
20. S. Lourdudoss et al., Proc. SPIE **10107**, 05 (2017)
21. Y. Özen et al., Solar Energy Mater. Solar Cells **137**, 1 (2015)
22. F. Lan et al., IEEE J. Photovolt. **8**, 125 (2018)
23. Z.M. Ma et al., Nanoscale Res. Lett. **8**, 532 (2013)
24. C. Marchat et al., Nanoscale Res. Lett. **14**, 398 (2019)
25. L. Kronik et al., Surf. Sci. Rep. **37**, 1 (1999)
26. L. Kronik et al., Chem. Electr. Eng. **31**, 954 (2000)

27. C. Baumgart et al., Phys. Rev. B **80**, 085305 (2009)
28. H.O. Jacobs et al., J. Appl. Phys. **84**, 1168 (1998)
29. R. Fornari et al., in International Conference on Indium Phosphide and Related Materials (2005), pp. 649–652
30. SILVACO® ATLAS™ User's Manual (2016)
31. Z. Zhang et al., Chem. Rev. **112**, 5520 (2012)
32. X. Sun et al., Opt. Mater. **7**, 904 (2017)
33. C. Marchat, Caractérisation électrique et optoélectronique de nouveaux matériaux et composants photovoltaïques à partir de techniques AFM, Université Paris-Saclay, 2020

Cite this article as: Mattia da Lisca, James P. Connolly, José Alvarez, Karim Mekhazni, Nicolas Vaissiere, Jean Decobert, Jean-Paul Kleider, Revealing of InP multi-layer stacks from KPFM measurements in the dark and under illumination, EPJ Photovoltaics **13**, 19 (2022)